

# InP-Based Passive Ring-Resonator-Coupled Lasers

Zhixi Bian, *Student Member, IEEE*, Bin Liu, *Member, IEEE*, and Ali Shakouri, *Member, IEEE*

**Abstract**—Design of passive ring-coupled lasers based on InGaAsP waveguides is investigated using beam propagation method. Mode coupling, propagation loss due to bending, and scattering loss from waveguide sidewall roughness are taken into account. By compromising threshold gain, linewidth and side-mode suppression ratio (SMSR), suitable waveguide width and coupling strength are determined for different ring sizes. Using a ring with radius ranging from 20 to 200  $\mu\text{m}$ , it is possible to design passive ring-coupled lasers with threshold gain less than 60/cm and 80/cm for waveguide sidewall roughness 5 and 10 nm, respectively, SMSR larger than 50 dB, and linewidth in the range of  $\sim 3$ –500 kHz.

**Index Terms**—Beam-propagation method, directional coupler, linewidth, microring resonators, side-mode suppression ratio, threshold gain, tunable lasers.

## I. INTRODUCTION

MICRORING resonators are of increasing interest. They are potential candidates for large-scale photonic integrated circuits for applications such as optical add/drop filters [1]–[6], signal processing, switching, modulation [7]–[10], and wavelength conversion [11]. This is due to their merits both as compact devices and as high Q resonators. Researchers studied the transmission characteristic of microrings by scattering matrix theory [1] and concluded that their performance is determined by two major parameters, coupling strength between straight waveguides and microrings, and microring round-trip loss. In the configuration of racetrack, coupling strength could be adjusted by changing gap size, coupling region length, or etch depth [12]. In order to make the free spectral range (FSR) large, a small radius of curvature microring is needed. Generally, a large refractive index contrast ridge waveguide structure is used to get the strong optical confinement, which is necessary to avoid large bending loss in the microrings. The deep etching to make such large refractive index contrast structures is a challenge. But state-of-the-art fabrication techniques have made this successful in both GaAs [13], [14] and InP [15], [16] based structures. Recently, a novel passive microring coupled laser [17] was proposed. In this structure, the effective cavity length can be extended considerably, making the photon lifetime much longer. This is the biggest difference between the passive ring-resonator-coupled lasers and the conventional active ring and Fabry–Perot (F–P) lasers. In ring lasers, the traveling-wave ring resonator replaces the standing wave F–P cavity and the cavity loss is due to the coupling between the

ring and the output waveguides. Therefore, to increase the photon lifetime, one must increase the physical length of the ring and/or reduce the coupling. These will be limited by the device size and the output power. However, in the case of passive ring-resonator-coupled lasers, the ring resonator is used as a passive mode selector. Thus, a frequency-dependent passive mirror with complex amplitude reflectivity is formed by the combination of a coupled microring resonator with a reflection facet. This frequency-dependent passive mirror can considerably extend the effective cavity length and photon lifetime at the lasing wavelength. Thus, the laser linewidth and the frequency chirp can be greatly reduced. In addition, a double-ring resonator configuration can be used to extend the wavelength tuning range greatly [18].

In passive microring coupled lasers, the threshold gain, linewidth and side-mode suppression ratio (SMSR) depend very much on the characteristics of the coupled microring. In this paper, we investigated InP-based ridge waveguide passive ring coupled lasers (RCLs) using beam-propagation method (BPM). The BPM is a simple and fast simulation approach suitable for paraxial propagation in waveguides. A conformal transformation method [19] could be applied in BPM to deal with the problem of curved waveguides and microring loss. We used BPM<sup>1</sup> to simulate scattering loss in straight waveguides, scattering and bending loss in microring, coupling loss between straight and curved waveguides in a racetrack configuration, and finally, the coupling coefficient  $k$  between parallel waveguides. Various parameters such as coupling gap size, coupling region length, microring radius of curvature, waveguide width, and thickness of waveguide layers were optimized in order to get maximum throughput and large finesse. The effects of imperfections such as waveguide sidewall roughness were also studied. Finally, the threshold gain, linewidth, and SMSR of passive-ring-coupled lasers were calculated.

## II. DESIGN OF PASSIVE RCL

A schematic diagram of passive RCL with racetrack configuration is depicted in Fig. 1. A laser cavity is formed with a combination of an active waveguide, passive waveguides, reflective facets, and the microring. The absorption region is introduced in order to reduce the reflections from other facets in the structure. The microring resonator is composed of two curved sections and two straight sections. The straight sections in the microring are laterally coupled to two parallel passive waveguides. One of the straight waveguides out of the microring is directly coupled to an active waveguide, which is typically a separate confinement hetero-structure p–i–n junction with quantum wells in the depletion region. The high Q ring works as a mode selection filter

Manuscript received October 16, 2002; revised December 12, 2002.

Z. Bian and A. Shakouri are with the Jack Baskin School of Engineering, University of California, Santa Cruz, CA 95064 USA (e-mail: ali@soe.ucsc.edu).

B. Liu is with the Department of Electrical and Computer Engineering, University of California, Santa Barbara, CA 93106 USA.

Digital Object Identifier 10.1109/JQE.2003.813222

<sup>1</sup>Rosft Inc., BeamPROP Version 5.0.

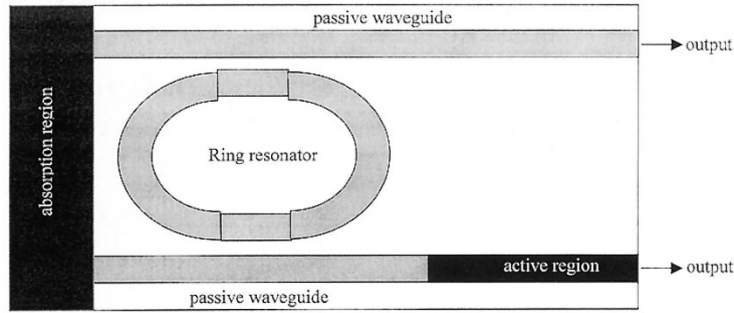


Fig. 1. Schematic of a passive RCL used for simulations.

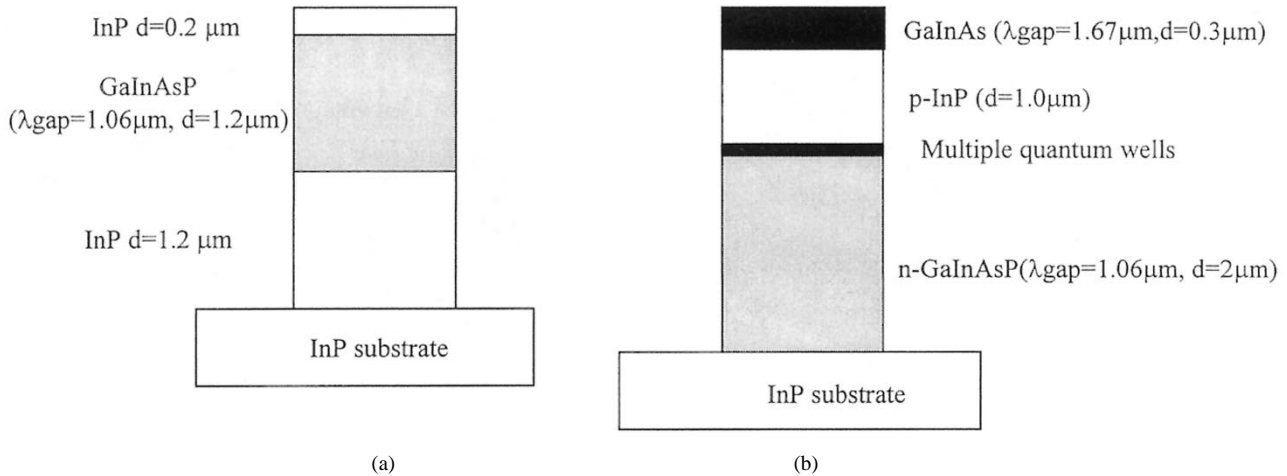


Fig. 2. Schematic of (a) passive waveguide and (b) active waveguide of RCL in used in the simulations.

and an external cavity. The reflectivity and transmittance of the mirrors are  $r_{11}$ ,  $t_{11}$ ,  $r_{22}$ , and  $t_{22}$ , respectively. The coupling coefficients between the passive waveguides and the ring are  $k_1$  and  $k_2$ . We use a design with  $k_1 = k_2 = k$  because symmetric coupling will optimize the tradeoff between linewidth and threshold.  $l_r$ ,  $\beta_r$ , and  $\alpha_r$  are the total length, the propagation constant, and the energy loss coefficient of the curved waveguides, respectively.  $L_c$ ,  $\beta_c$ , and  $\alpha_c$  are the length, the propagation constant, and the energy loss coefficient of the straight sections of the ring and the straight outer waveguides, respectively. In our model, we assume that  $\beta_r = \beta_c = \beta$ . There are four joints inside the ring where coupling loss between straight and curved waveguides can occur due to mode mismatch. This is represented by mode energy coupling  $T_p$ .  $T_a$  represents the transfer of energy between passive straight waveguide and active region.  $l_g$  is the length of the gain section. The transmission characteristics of the ring, such as transmission amplitude, phase, and finesse, will affect threshold gain, mode spacing, SMSR, linewidth, and tunability of the RCL. The transmission characteristics are in turn determined by the coupling coefficients between the microring and outer waveguides, and mode mismatch and transmission loss in the microring. In this paper, we investigate theoretically how the coupling coefficients  $k$  and losses depend on fabrication parameters such as waveguide width, gap size in the coupling region, coupling length, ring's radius of curvature, offset between straight and curved waveguides, and surface roughness due to wet or dry etching.

The schematic cross-section of passive and active waveguides is shown in Fig. 2. The layer sequence of passive waveguides and microring starting from the substrate is as follows: InP substrate ( $n = 3.168$ ), InP cladding layer ( $1.2 \mu\text{m}$ ), GaInAsP core layer ( $\lambda_{\text{gap}} = 1.06 \mu\text{m}$ ,  $1.2 \mu\text{m}$ ), InP cap ( $0.2 \mu\text{m}$ ). Several waveguide widths are investigated to see the loss dependence. A structure with high optical confinement is used in order to reduce bending loss in microring. The layer sequence of active region is as follows: InP substrate, n-GaInAsP ( $\lambda_{\text{gap}} = 1.06 \mu\text{m}$ ,  $2\text{-}\mu\text{m}$  thickness), six quantum wells, and five barriers ( $\lambda_{\text{gap}} = 1.29 \mu\text{m}/1.55 \mu\text{m}$ , thickness  $8 \text{ nm}/8 \text{ nm}$ ), p-InP ( $1.0 \mu\text{m}$ ), GaInAs cap ( $0.3 \mu\text{m}$ ).

### III. MICRORING MODEL

The overall performance of RCL depends strongly on the characteristics of the microring. In a microring with a given size, coupling strength with outer waveguides and loss in the ring will determine the transmission characteristic. It is easy to derive the electric field transfer function of the racetrack microring using scattering matrix method

$$t = \frac{-k_1 k_2 T_p \exp(i\beta(2l_c + \frac{l_r}{2})) \exp(-\alpha_c l_c) \exp(\frac{-\alpha_r l_r}{4})}{1 - t_1 t_2 T_p^2 \exp(i\beta(l_r + 2l_c)) \exp(-\alpha_c l_c) \exp(\frac{-\alpha_r l_r}{2})} \quad (1)$$

where

$$t_1^2 + k_1^2 = 1, \quad t_2^2 + k_2^2 = 1. \quad (2)$$

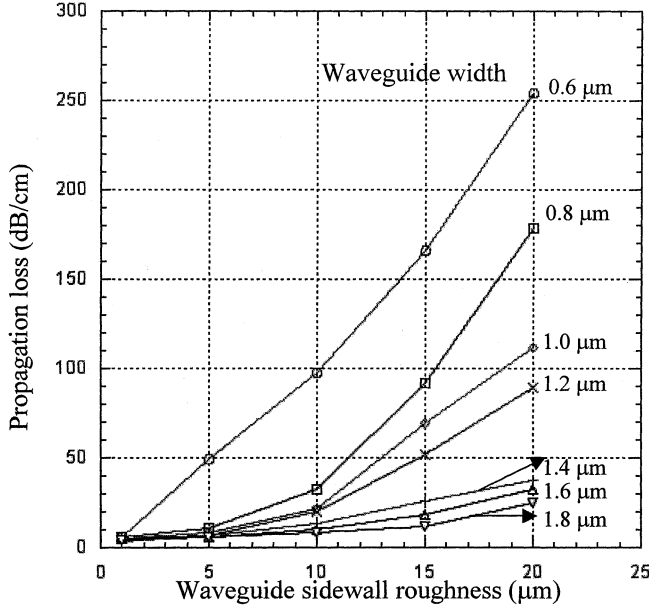


Fig. 3. Propagation loss for straight waveguides.

From the amplitude transfer function, it can be seen that at resonant frequency, the power transmission reaches its maximum. The power transmission at resonance is an important factor for RCL because it is related to the lasing modes' total loss. The power transmission at resonance is

$$T_{r \max} = \left[ \frac{k_1 k_2 T_p \exp(-\alpha_c l_c) \exp\left(\frac{-\alpha_r l_r}{4}\right)}{1 - t_1 t_2 T_p^2 \exp(-\alpha_c l_c) \exp\left(\frac{-\alpha_r l_r}{2}\right)} \right]^2. \quad (3)$$

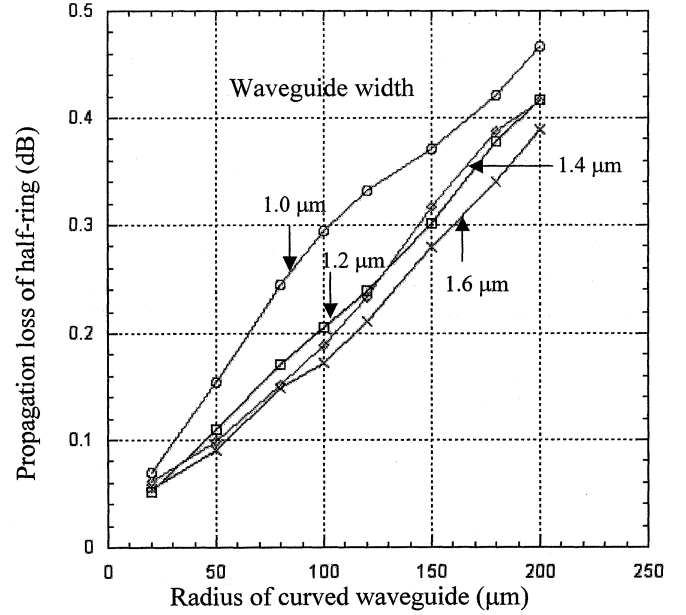
Finesse of the microring is an important factor that shows the filtering quality, which limits the SMSR of the RCL. Finesse depends on coupling coefficients and loss as

$$F_r = \pi \sqrt{\frac{t_1 t_2 T_p^2 \exp(-\alpha_c l_c) \exp\left(\frac{-\alpha_r l_r}{2}\right)}{[1 - t_1 t_2 T_p^2 \exp(-\alpha_c l_c) \exp\left(\frac{-\alpha_r l_r}{2}\right)]^2}}. \quad (4)$$

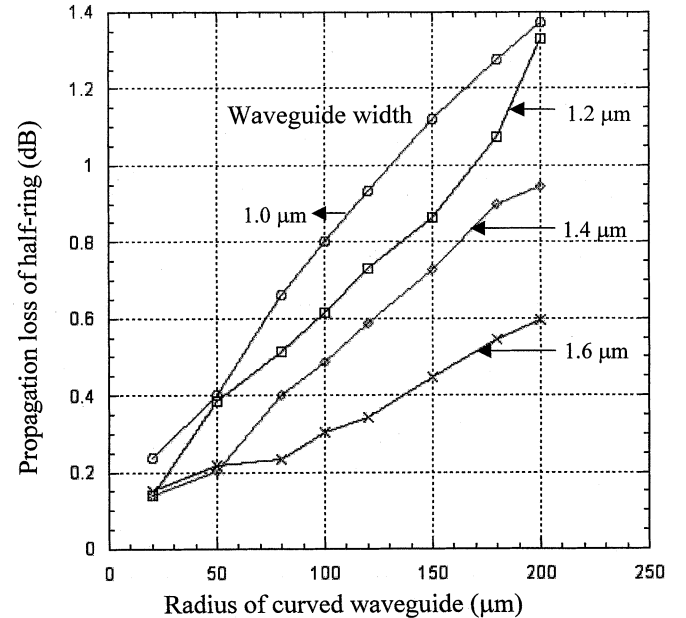
RCLs have low threshold, narrow linewidth, and high SMSR when the overall transmission at resonance and finesse of the microring are high. This can be achieved only with very small loss. There is a tradeoff between transmission at resonance and its finesse, which is determined by coupling strength  $k$ . In our simulation, we want to find a range of device parameters that give small loss and suitable coupling coefficients.

#### IV. SIMULATIONS

Simulations show that straight passive waveguides with widths ranging from 0.6 to 1.6  $\mu\text{m}$  were single mode at 1.55- $\mu\text{m}$  wavelength. In the straight passive waveguides with high-index contrast, the propagation loss is dominated by the scattering loss due to the sidewall roughness of the waveguides. Quantitatively, the scattering loss is proportional of the root mean square of surface roughness, the index difference between the core and cladding, and the field intensity at the interface. The waveguide width and sidewall roughness dependences of the propagation loss of straight waveguides are shown in Fig. 3. The propagation loss increases monotonically with the sidewall



(a)



(b)

Fig. 4. Propagation loss of curved waveguides with sidewall roughness (a) 5 nm and (b) 10 nm.

roughness. The propagation loss and its sensitivity on waveguide sidewall roughness are smaller for a wider waveguide. In the following, single-mode waveguides with 1.0-, 1.2-, 1.4-, and 1.6- $\mu\text{m}$  widths will be used in the simulations.

Since the loss in the microring degrades its transmission and filtering quality considerably as shown in (3) and (4), it was studied in detail. The propagation loss for half of the microring is shown in Fig. 4 (a) and (b) for waveguide sidewall roughness of 5 and 10 nm, respectively. It can be seen that the loss is almost proportional to ring size and that wider waveguide microrings have smaller loss. Because the mode intensity shifts to outer surfaces in curved waveguides, there will be a mode-coupling loss

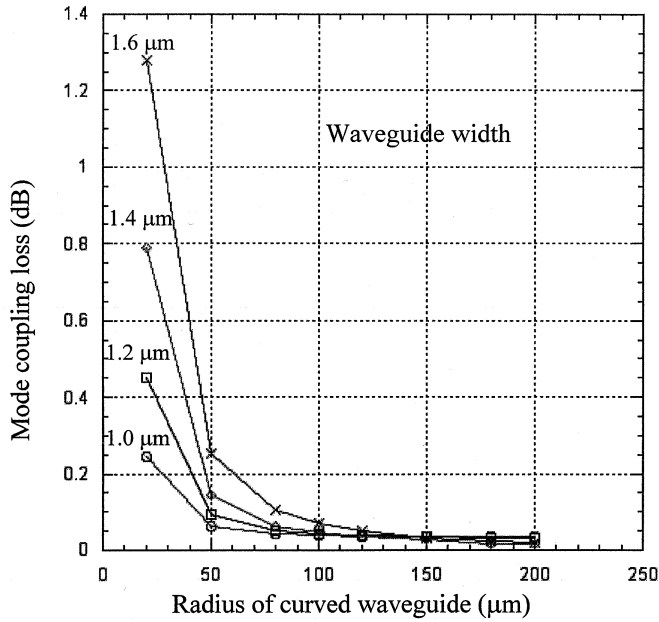


Fig. 5. Mode-coupling loss between straight and curved waveguides.

between straight and curved sections, as shown in Fig. 5. It can be seen that the smaller the radius of curvature or waveguide width, the larger the mode-coupling loss is. This is because the mode mismatch between the straight and curved waveguides increases with the decrease of the radius. The coupling loss also strongly depends on the waveguide width. With a narrow waveguide, the coupling loss can be substantially reduced for small radius. This is due to the fact that the mode shift is reduced and the mode match is improved in narrow waveguides. To reduce this coupling loss, one can introduce a lateral offset between the straight and the curved waveguides to minimize the mode mismatch. To study the microring with different FSR, microring radius of 20, 50, 100 and 200  $\mu\text{m}$  will be used in the simulation. For these four radii, waveguide widths of 1.0, 1.2, 1.4, and 1.6  $\mu\text{m}$  are good candidates, respectively, to reduce the total ring loss. The total loss, which includes the propagation loss in the ring resonators and two mode-coupling losses, for these four candidates, is shown in Fig. 6.

Since there are losses in the microring, transmission at resonance will not be unity. Coupling coefficients between the ring and outer waveguide can be increased to compensate the loss in microring, which will improve transmission but degrade Q factor. Suitable coupling coefficients can be chosen by compromising between transmission and Q factor. Coupling strength depends on coupling length, gap size, and waveguide width. The gap size dependence of coupling coefficient  $k$  is shown in Fig. 7 for waveguide width 1.4  $\mu\text{m}$ . It can be seen that the coupling coefficient is very sensitive to gap size. Generally, long coupling length is not preferred, because this can increase the overall scattering loss in the ring. Zero gap size is a good choice because the coupling length is less than 15  $\mu\text{m}$  for a coupling coefficient less than 0.3, which is much smaller than total ring length. Another merit of zero gap size is that it is easier to fabricate and it is not sensitive to fabrication variations. Dependence of amplitude coupling coefficients on coupling length for different waveguide

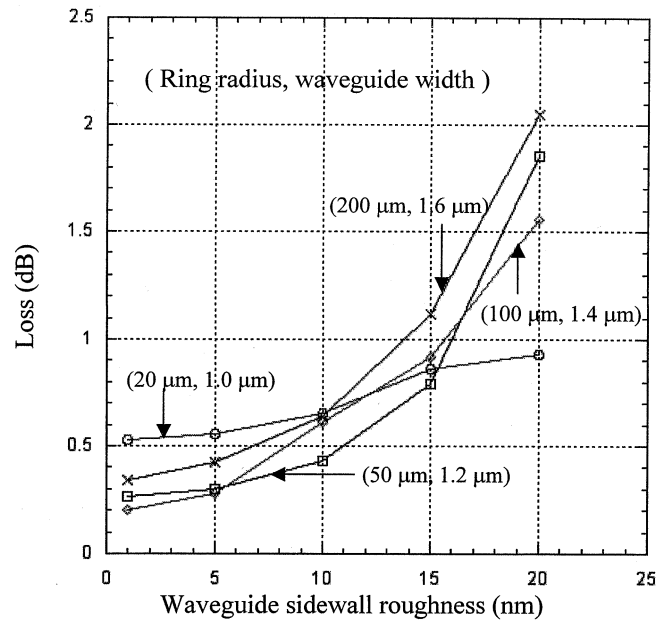


Fig. 6. Total loss of half-ring, including sidewall scattering loss and two mode-coupling losses.

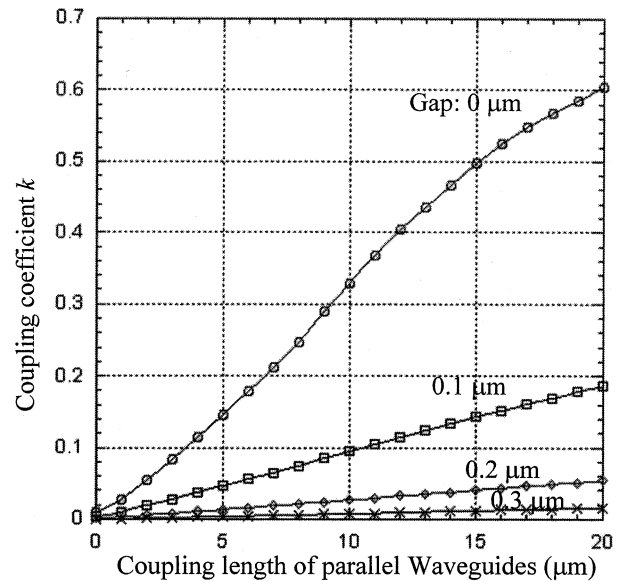


Fig. 7. Coupling coefficients between two straight waveguides for different gap sizes.

widths is shown in Fig. 8. Narrower waveguides have stronger coupling. These curves will be used to look for the optimal coupling length in the tradeoff among the threshold gain, SMSR, and linewidth of the RCL.

In our design, loss due to mode mismatch between passive and active waveguides is included in calculations. The thickness of n region in the active waveguide is adjusted to minimize mode-coupling loss. The optimal thickness of the n region is 2.0  $\mu\text{m}$  and the maximum mode coupling is 87%. In our final calculations, we will assume the total loss of active region, including waveguide sidewall and impurity scattering, is 20/cm.

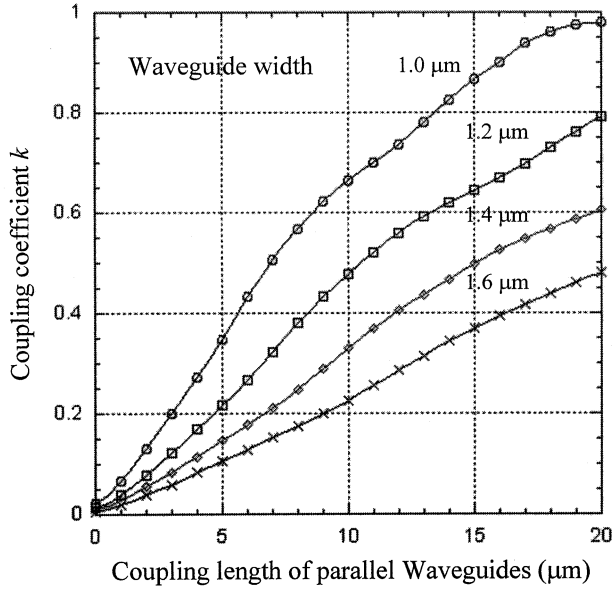


Fig. 8. Coupling coefficients for different waveguide widths.

### V. CALCULATIONS

The transmission characteristic of microring is comb-like. Its FSR is as follows:

$$\text{FSR} = \frac{\lambda^2}{(n_r l_r + 2n_w l_c)}. \quad (5)$$

In the case of zero gap size, straight sections are short compared to curved ones in the microring. Thus, FSR is mainly determined by the radius of curvature of microring. We use radius of 20, 50, 100, and 200  $\mu\text{m}$  to meet the different needs of the FSR.

The threshold gain of RCL in this design depends on mode coupling between passive and active waveguides and transmission at resonance

$$g_{\text{th}} = \alpha_g + \frac{1}{l_g} \ln \left( \frac{1}{r_{11} r_{22} T_w T_r T_a} \right) \quad (6)$$

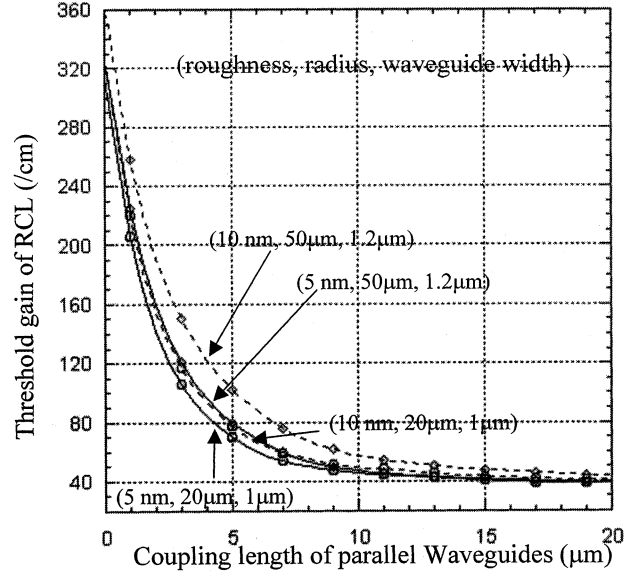
where  $T_w$  is the energy transmittance of the passive waveguides out of the microring. The thresholds of the four candidates with waveguide sidewall roughness of 5 and 10 nm are plotted in Fig. 9. Here, we assume total loss in gain region is 20 /cm, amplitude reflectivity at facets is 0.8 by coating, length of gain section is 400  $\mu\text{m}$ , total length of passive waveguide out of microring is 100  $\mu\text{m}$ , effective refractive index of active waveguide is 3.3, effective refractive index of all passive region is 3.2, and coupling between active and passive region is 0.87.

Both the linewidth and SMSR of RCL depend on mode spacing. Mode spacing is given by

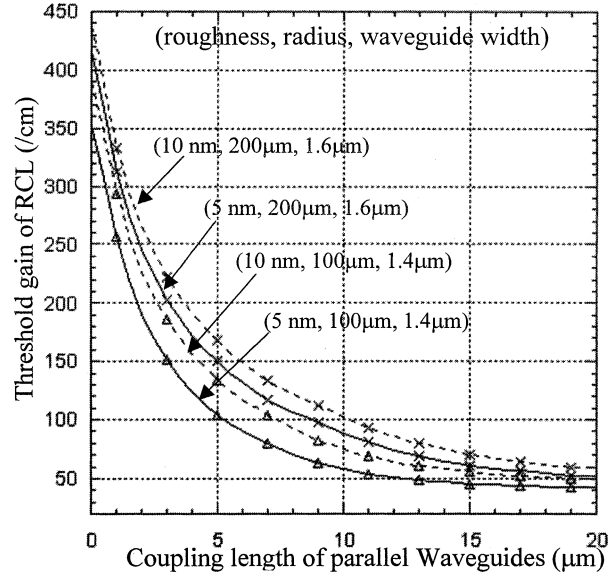
$$\delta\lambda_m = \frac{\lambda^2}{2(n_w l_w + n_r l_{\text{eff}} + n_g l_g)} \quad (7)$$

where effective ring length can be derived from the phase of microring transmission function

$$\begin{aligned} l_{\text{eff}} &= \frac{\partial\theta}{\partial\beta} \\ &= \left( \frac{2l_c + l_r}{2} \right) + \frac{t_1 t_2 T_p^2 \exp(-\alpha_c l_c) \exp\left(\frac{-\alpha_r l_r}{2}\right)}{1 - t_1 t_2 T_p^2 \exp(-\alpha_c l_c) \exp\left(\frac{-\alpha_r l_r}{2}\right)} \\ &\quad \times (2l_c + l_r). \end{aligned} \quad (8)$$



(a)



(b)

Fig. 9. Threshold gain of RCL with waveguide sidewall roughness 5 nm (solid lines) and 10 nm (dashed lines). (a) Ring radius 20  $\mu\text{m}$ , waveguide width 1.0  $\mu\text{m}$ ; and ring radius 50  $\mu\text{m}$ , waveguide width 1.2  $\mu\text{m}$ . (b) Ring radius 100  $\mu\text{m}$ , waveguide width 1.4  $\mu\text{m}$ ; and ring radius 200  $\mu\text{m}$ , waveguide width 1.6  $\mu\text{m}$ .

The passive RCL has the merits of high SMSR and very narrow linewidth thanks to the high Q ring. This is very useful in the coherent communication or for spectroscopic applications. The power output ratio of the main mode to the first side mode  $\chi$  is given by [20]

$$\chi = \frac{2n_g P_0}{h\nu n_{\text{sp}} \gamma_{\text{tot}}} \left[ \frac{\Delta\gamma l_g}{\gamma_m l_g} \right] \quad (9)$$

and the SMSR is

$$\text{SMSR} = 10 \log(\chi) \quad (10)$$

Here,  $P_0$  is the output power,  $n_{\text{sp}}$  is the spontaneous emission factor with typical value around 2,  $\gamma_{\text{tot}}$  is the total loss,  $\gamma_m$  is the mirror loss, and  $\Delta\gamma$  is the loss difference between the main

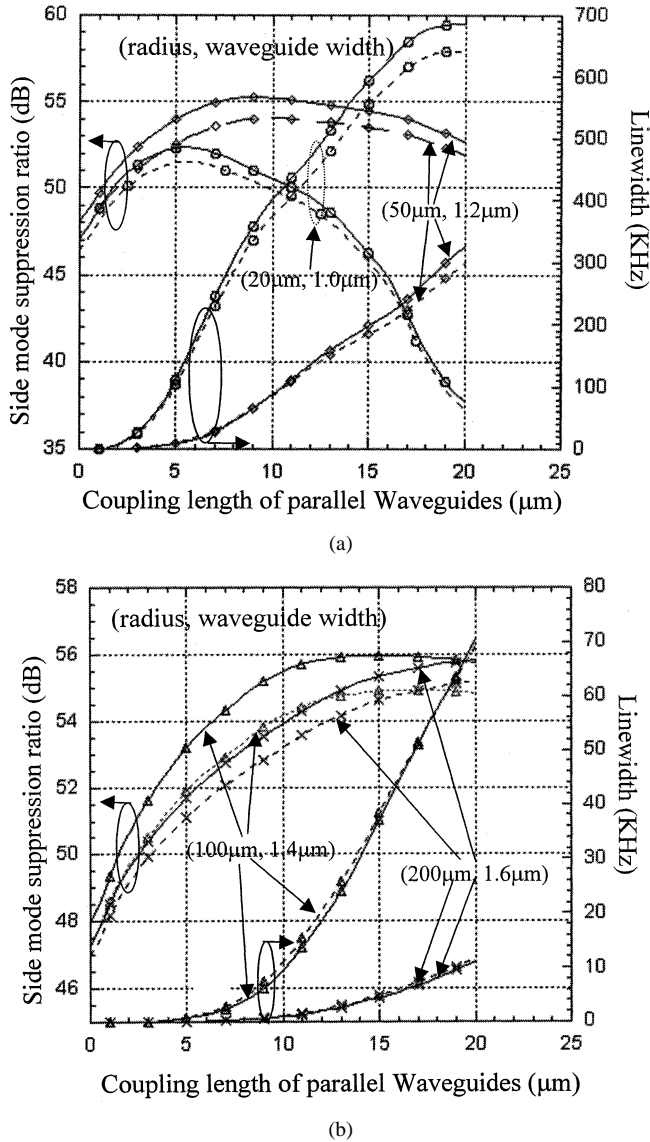


Fig. 10. SMSR and linewidth of RCL with waveguide sidewall roughness 5 nm (solid lines) and 10 nm (dashed lines). (a) Ring radius 20  $\mu\text{m}$ , waveguide width 1.0  $\mu\text{m}$ ; and ring radius 50  $\mu\text{m}$ , waveguide width 1.2  $\mu\text{m}$ . (b) Ring radius 100  $\mu\text{m}$ , waveguide width 1.4  $\mu\text{m}$ ; and ring radius 200  $\mu\text{m}$ , waveguide width 1.6  $\mu\text{m}$ .

mode and the first side mode. In the case of the RCL, the loss difference is given by

$$\begin{aligned} \Delta\gamma * l_g &= \ln \frac{T_r \max}{T_r(\delta\lambda_m)} \\ &= \ln \left[ 1 + \left( \frac{2F_r}{\pi} \right)^2 \sin^2 \left( \pi \frac{2n_w l_c + n_r l_r}{\lambda^2} \delta\lambda_m \right) \right] \end{aligned} \quad (11)$$

where the mode spacing is shown in (7). It is obvious that high  $Q$  will benefit the SMSR.

The linewidth of passive RCL is given by [17]

$$\begin{aligned} \Delta\nu &= \Delta\nu_0 \left( \frac{n_g l_g}{n_g l_g + n_r l_{\text{eff}} + n_w l_w} \right)^2 \\ &\times \frac{2r_{11} T_w T_r T_a (1 - r_{22}^2)}{(r_{11} T_w T_r T_a + r_{22})(1 - r_{11} T_w T_r T_a r_{22})}. \end{aligned} \quad (12)$$

TABLE I

SOME DESIGNS FOR RCL WITH SIDEWALL ROUGHNESS LESS THAN 5 nm, THRESHOLD GAIN LESS THAN 60/cm, SIDEWALL ROUGHNESS LESS THAN 10 nm, AND THRESHOLD GAIN LESS THAN 80/cm

Sidewall roughness (nm)	Width, ring radius ( $\mu\text{m}$ )	Coupling length range ( $\mu\text{m}$ )	Threshold gain (1/cm)	SMSR range (dB)	Linewidth range (KHz)
<5	1.0, 20	[6, 11]	[59.7, 44.5]	[52.3, 50]	[178, 436]
	1.2, 50	[7, 20]	[59.5, 38.9]	[54.9, 52.6]	[28, 327]
	1.4, 100	[10, 20]	[57.7, 42.1]	[55.5, 55.7]	[9.5, 70.4]
	1.6, 200	[15.5, 20]	[59.8, 51.5]	[55.4, 55.8]	[5, 11]
<10	1.0, 20	[5, 9.5]	[78.1, 50.3]	[51.4, 50.1]	[103, 358]
	1.2, 50	[7, 20]	[75.9, 43.3]	[53.5, 51.8]	[29.6, 299]
	1.4, 100	[9.5, 20]	[78.4, 49.2]	[54, 54.8]	[9.1, 69.4]
	1.6, 200	[13, 20]	[79.6, 58.1]	[54, 55]	[3, 11.6]

$\Delta\nu_0$  is the linewidth of solitary laser given by

$$\Delta\nu_0 = \frac{1}{8\pi} \frac{v_g^2 \hbar \omega n_{\text{sp}} \gamma_{\text{tot}} \gamma_m (1 + \alpha^2)}{P_0} \quad (13)$$

where  $\alpha$  is the linewidth enhancement factor with typical value around 6 for bulk InGaAsP lasers.

Both the SMSR and linewidth of RCL for the four candidates with waveguide sidewall roughness of 5 and 10 nm are plotted in Fig. 10. In Figs. 9 and 10, it can be seen that the effects of sidewall roughness are smaller for the candidates with waveguide widths 1.0  $\mu\text{m}$  and 1.6  $\mu\text{m}$  than those with waveguide widths 1.2 and 1.4  $\mu\text{m}$ . This is because the one with width 1.0  $\mu\text{m}$  has a short length and the one with width 1.6  $\mu\text{m}$  has a small sidewall roughness dependence of the propagation loss coefficient. In general, the threshold gain and linewidth increase with the coupling length, and the SMSR increases first then decrease when the coupling length increases. This is because transmission at resonance increases, photon life and effective length of the ring decrease, with the increasing coupling strength. If transmission at resonance increases, the threshold gain will become smaller, as will the total loss. If photon lifetime decreases, linewidth will become wider. As for SMSR, both the filter bandwidth of the microring and laser mode spacing become larger so that SMSR increases first and decreases later with increasing coupling strength as the loss margin between main mode and the first side mode. Thus, there is a tradeoff of coupling length among threshold gain, SMSR and linewidth. Some good designs are shown in Table I. It can be seen that there is a compromising among threshold gain, SMSR, and linewidth. For all these designs, SMSR greater than 50 dB and linewidth less than less than 500 kHz can be achieved. The threshold gain is less than 60/cm for 5-nm sidewall roughness and is less than 80/cm for sidewall roughness 10 nm.

## VI. SUMMARY

In conclusion, InP-based passive RCLs were designed and simulated. The designs can be optimized based on the needs on FSR, threshold gain, linewidth, and SMSR of RCLs. From simulations, a design with racetrack configuration, zero gap size, and high-confinement optical waveguide with appropriate width depending on ring size can meet the needs of threshold gain less than 60/cm for waveguide sidewall roughness of not greater than 5 nm or threshold gain less than 80/cm for waveguide sidewall roughness not greater than 10 nm, SMSR larger than 50 dB, and linewidth in the range of  $\sim 3$ –500 KHz.

## REFERENCES

- [1] K. Oda, N. Takato, and H. Toba, "A wide-FSR waveguide double-ring resonator for optical FDM transmission systems," *J. Lightwave Technol.*, vol. 9, pp. 728–736, June 1991.
- [2] S. T. Chu, B. E. Little, W. Pan, T. Kaneko, S. Sato, and Y. Kokubun, "An eight-channel add-drop filter using vertically coupled microring resonators over a cross grid," *IEEE Photon. Technol. Lett.*, vol. 11, pp. 691–693, June 1999.
- [3] G. Griffel, "Synthesis of optical filters using ring resonator arrays," *IEEE Photon. Technol. Lett.*, vol. 12, pp. 810–812, July 2000.
- [4] —, "Vernier effect in asymmetrical ring resonator arrays," *IEEE Photon. Technol. Lett.*, vol. 12, no. 12, pp. 1642–1644, Dec. 2000.
- [5] B. E. Little and S. T. Chu, "Theory of loss and gain trimming of resonator-type filters," *IEEE Photon. Technol. Lett.*, vol. 12, pp. 636–638, June 2000.
- [6] P. P. Absil, J. V. Hryniewicz, B. E. Little, R. A. Wilson, L. G. Joneckis, and P.-T. Ho, "Compact microring notch filters," *IEEE Photon. Technol. Lett.*, vol. 12, no. 4, pp. 398–400, Apr. 2000.
- [7] B. E. Little, H. A. Haus, J. S. Foresi, L. C. Kimerling, E. P. Ippen, and D. J. Ripin, "Wavelength switching and routing using absorption and resonance," *IEEE Photon. Technol. Lett.*, vol. 10, pp. 816–818, June 1998.
- [8] R. A. Soref and B. E. Little, "Proposed N-wavelength M-fiber WDM crossconnect switch using active microring resonators," *IEEE Photon. Technol. Lett.*, vol. 10, pp. 1121–1123, Aug. 1998.
- [9] V. Van, T. A. Ibrahim, K. Ritter, P. P. Absil, F. G. Johnson, R. Grover, J. Goldhar, and P.-T. Ho, "All-optical nonlinear switching in GaAs-AlGaAs microring resonators," *IEEE Photon. Technol. Lett.*, vol. 14, pp. 74–76, Jan. 2002.
- [10] A. Yariv, "Critical coupling and its control in optical waveguide-ring resonator systems," *IEEE Photon. Technol. Lett.*, vol. 14, pp. 483–485, Apr. 2002.
- [11] P. P. Absil, J. V. Hryniewicz, B. E. Little, P. S. Cho, R. A. Wilson, L. G. Joneckis, and P.-T. Ho, "Wavelength conversion in GaAs micro-ring resonators," *Opt. Lett.*, vol. 25, no. 8, pp. 554–556, Apr. 15, 2000.
- [12] G. Griffel, J. H. Abeles, R. J. Menna, A. M. Braun, J. C. Connolly, and M. King, "Low-threshold InGaAsP ring lasers fabricated using bi-level dry etching," *IEEE Photon. Technol. Lett.*, vol. 12, pp. 146–148, Feb. 2000.
- [13] V. Van, P. P. Absil, J. V. Hryniewicz, and P.-T. Ho, "Propagation loss in single-mode GaAs-AlGaAs microring resonators: measurement and model," *J. Lightwave Technol.*, vol. 19, no. 11, pp. 1734–1739, Nov. 2001.
- [14] D. Rafizadeh, J. P. Zhang, R. C. Tiberio, and S. T. Ho, "Propagation loss measurements in semiconductor microcavity ring and disk resonators," *J. Lightwave Technol.*, vol. 16, no. 7, pp. 1308–1314, July 1998.
- [15] D. G. Rabus and M. Hamacher, "MMI-coupled ring resonators in GaInAsP-InP," *IEEE Photon. Technol. Lett.*, vol. 13, pp. 812–814, Aug. 2001.
- [16] R. Grover, P. P. Absil, V. Van, J. V. Hryniewicz, B. E. Little, O. King, L. C. Calhoun, F. G. Johnson, and P.-T. Ho, "Vertically coupled GaInAsP-InP microring resonators," *Opt. Lett.*, vol. 26, no. 8, pp. 506–508, Apr. 15, 2001.
- [17] B. Bin Liu, A. Shakouri, and J. E. Bowers, "Passive microring-resonator-coupled lasers," *Appl. Phys. Lett.*, vol. 79, no. 22, pp. 3561–3563, Nov. 26, 2001.
- [18] —, "Wide tunable double ring resonator coupled lasers," *IEEE Photon. Technol. Lett.*, vol. 14, pp. 600–602, May 2002.
- [19] M. K. Chin and S. T. Ho, "Design and modeling of waveguide-coupled single-mode microring resonators," *J. Lightwave Technol.*, vol. 16, pp. 1433–1446, Aug. 1998.
- [20] T. L. Koch and U. Koren, "Semiconductor lasers for coherent optical fiber communications," *J. Lightwave Technol.*, vol. 8, pp. 274–293, Mar. 1990.

**Zhixi Bian** (SM'03) received the B.S. degree from Nankai University, Nankai, China, in 1993, and the M.S. degree from Beijing University, China, in 1996. He is currently working toward the Ph.D degree at the University of California at Santa Cruz.

His research includes the design, simulation, and fabrication of tunable semiconductor lasers and electroabsorption modulators.

**Bin Liu** (M'98) received the B.S. degree from Zhejiang University, Zhejiang, China, in 1990, the M.S. degree from Shanghai Institute of Optics and Fine Mechanics, Chinese Academy of Science, Shanghai, China, in 1995, and the Ph.D degree in electrical Engineering from the University of California at Santa Barbara in 2000.

His research interests include the design and fabrication of semiconductor optical waveguide devices, lasers, photonic integrated circuits, and microoptic devices.

**Ali Shakouri** (M'98) received the degree in engineering from Ecole Nationale Supérieure des Telecommunications de Paris, France, in 1990, and the Ph.D. degree from California Institute of Technology, Pasadena, in 1995. His dissertation was on electron transport in quantum-well infrared photodetectors.

He is currently an Associate Professor in the Electrical Engineering Department, University of California at Santa Cruz. His present research is in photonic integrated-circuit design and fabrication, integrated cooling of electronic devices, thermal imaging, heat and current transport in micro and nano-structures, and molecular beam epitaxy.